Deterministic Integration of Single Photon Sources in Silicon Based Photonic Circuits

Zadeh, Iman Esmaeil; Elshaari, Ali W.; Jöns, Klaus D.; Fognini, Andreas; Dalacu, Dan; Poole, Philip J.; Reimer, Michael E.; Zwiller, Val

DOI
10.1021/acs.nanolett.5b04709

Publication date
2016

Document Version
Final published version

Published in
Nano Letters: a journal dedicated to nanoscience and nanotechnology

NANO LETTERS

Letter

pubs.acs.org/NanoLett

Deterministic Integration of Single Photon Sources in Silicon Based Photonic Circuits

Iman Esmaeil Zadeh,[*,†,⊥] Ali W. Elshaari,[*,†,‡,⊥] Klaus D. Jöns,[†,‡] Andreas Fognini,[†] Dan Dalacu,[§] Philip J. Poole,[§] Michael E. Reimer,[∥] and Val Zwiller[†,‡]

[†]Kavli Institute of Nanoscience Delft, Delft University of Technology, Delft 2628 CJ, The Netherlands

[‡]Department of Applied Physics, Royal Institute of Technology (KTH), Stockholm 106 91, Sweden

[§]National Research Council of Canada, Ottawa, ON K1A 0R6, Canada

[∥]Institute for Quantum Computing and Department of Electrical & Computer Engineering, University of Waterloo, Waterloo, ON N2L 3G1, Canada

Supporting Information

ABSTRACT: A major step toward fully integrated quantum optics is the deterministic incorporation of high quality single photon sources in on-chip optical circuits. We show a novel hybrid approach in which preselected III−V single quantum dots in nanowires are transferred and integrated in silicon based photonic circuits. The quantum emitters maintain their high optical quality after integration as verified by measuring a low multiphoton probability of 0.07 ± 0.07 and emission line width as narrow as 3.45 ± 0.48 GHz. Our approach allows for optimum alignment of the quantum dot light emission to the fundamental waveguide mode resulting in very high coupling efficiencies. We estimate a coupling efficiency of 24.3 ± 1.7% from the studied single-photon source to the photonic channel and further show by finite-difference time-domain simulations that for an optimized choice of material and design the efficiency can exceed 90%.

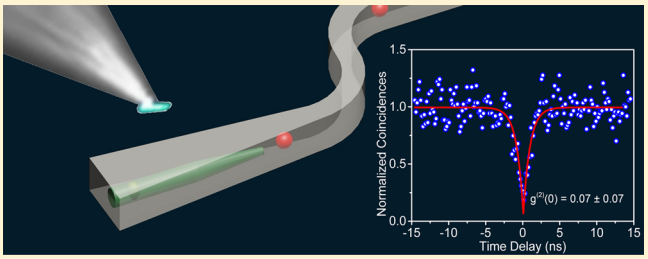

KEYWORDS: *Integrated quantum optics, nanowire quantum dot, single-photons, hybrid photonics*

Experiments on photons have played a key role in our understanding of quantum mechanics by probing the quantized nature of electromagnetic radiation. Since Linear Optical Quantum Computing (LOQC)[1] was proposed, there has been an ongoing effort to achieve a scalable platform for its realization. Few qubit operations have been shown[2,3] and up to eight photon entanglement has been achieved[4] using discrete optical components and parametric down conversion. Although many basic proof of principles have been demonstrated, a more scalable approach is needed for complex architectures. Recently, integrated photonics has gained significant interest as it offers scalability, robustness, and ease of use for on-chip quantum computation.[5−9]

A LOQC system comprised of three main components: single photon generation, manipulation, and detection. Single-photons used in integrated photonic circuits are often generated using parametric down conversion or quantum dots (QD). As opposed to parametric down conversion, QDs are suitable for on-demand single photon generation[10] and narrow emission bandwidth, their emission wavelength can be tuned,[11−15] and they offer the possibility of on-chip electrical excitation.[16] As for the logical quantum gates, every discrete unitary operator can be realized using only mirrors and beam splitters.[17] This makes the integrated photonic platform very attractive due to the already available components for passive and active light manipulation.[18] In addition, for single photon detection, >90% system efficiency has been achieved.[19] However, to realize an efficient LOQC system, it is required to interface all of these often incompatible technologies.

Significant efforts have been put into realizing LOQC on-chip. For on-chip detection, efficient coupling of superconducting nanowire single-photon detectors (SNSPD) with dielectric waveguides has been demonstrated.[20,21] As for the gate operations, complex photonic circuits for quantum operations have been realized.[22,23] In addition, QDs have been coupled to photonic cavities, nanowires, waveguides,[24−26] and SNSPDs.[27] Fabricating low-loss III−V waveguides and selectively embedding single-quantum emitters is a challenge.[28,29] Moreover, growing superconducting films (for detectors) on these substrates often leads to low efficiency or high dark counts.[30]

In this work, we present a novel hybrid platform through integration of III−V preselected single QDs embedded in nanowires within robust SiN photonic circuits. Unlike the work with NV centers,[31] we embed sources with directional emissions that is perfectly suited for coupling to the

Received: November 19, 2015
Revised: February 26, 2016
Published: March 8, 2016

DOI: 10.1021/acs.nanolett.5b04709
Nano Lett. 2016, 16, 2289−2294

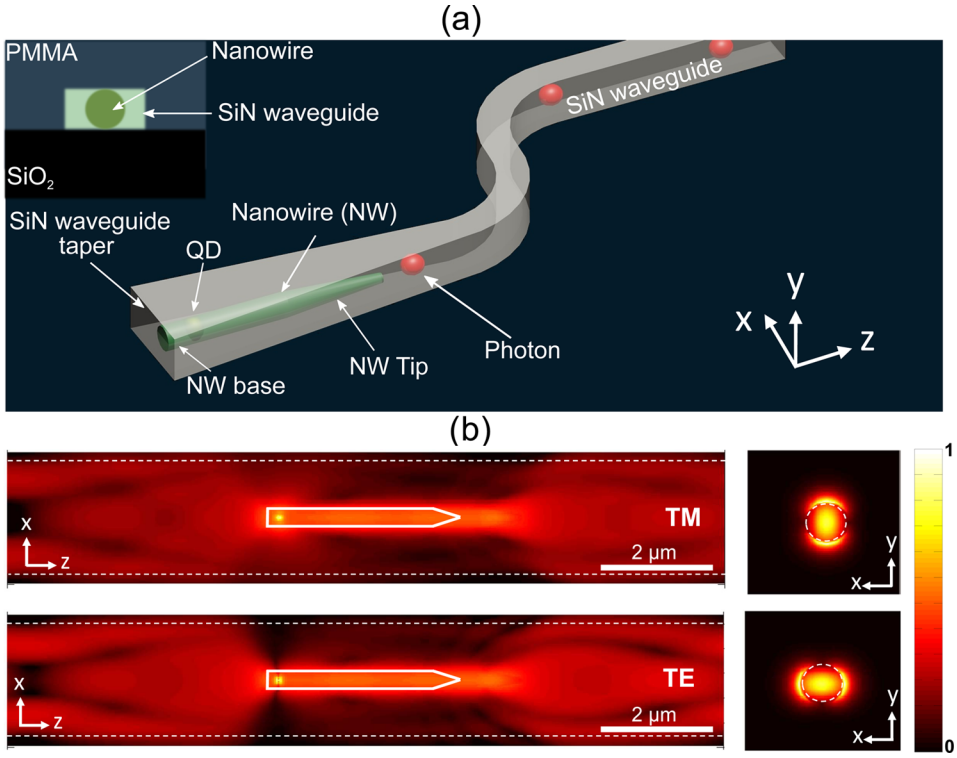

Figure 1. (a) Schematic view of the device, where a III−V QD in a nanowire is embedded in a SiN photonic waveguide. The emitted photons are depicted with red spheres propagating along the waveguide (only the forward direction is shown). (b) Three-dimensional FDTD simulations for the embedded QD emission at 880 nm. Horizontal cuts of the electric field profile are shown for both of the orthogonal polarization directions. The SiN waveguide boundaries are shown by the dashed lines. The insets show vertical cuts of the electric field intensity profile at the QD for both TE and TM modes. The total simulated coupling efficiency for unpolarized emission from the dot to the guided modes in the SiN waveguide is 36% (~18% for forward and backward directions).

waveguides. Figure 1a provides an artistic visualization of such an integrated quantum circuit element. The red spheres represent single photons that are coupled to the waveguide in the forward direction. The indium phosphide nanowires are 1.5−3 μm in length and 250−300 nm in diameter with a 3−4 nm section of indium arsenide phosphide, forming the QD, located 200 nm from their base. During growth, once the length of the nanowire is longer than the diffusion length of indium, it tapers with an angle depending on the growth parameters.[32] For the photonic channel, the waveguide height is 200 nm with a width of 2 μm near the nanowire region to simplify alignment during fabrication. The waveguide is then tapered adiabatically to 800 nm for single mode operation. The SiN layer is formed using plasma enhanced chemical vapor deposition (PECVD) with a measured refractive index of ~2 near the QD emission (see Supporting Information Note.1).

Our design allows for strong overlap of the QD electric dipole moment and the fundamental modes of the waveguide since the z-quantization axis of the QD is aligned along the propagation direction of the waveguide. The QD electric dipole moment lies in the X−Y plane and can generally be represented as a linear combination of the orthogonal transverse modes (TE and TM) supported by the photonic channel. Figure 1b shows finite-difference time-domain (FDTD) simulations of coupling from the nanowire QD to TM and TE modes. The insets illustrate the electric field intensity in the X-direction (TE mode) and Y-direction (TM mode). For the given waveguide and nanowire geometry, the theoretical QD to waveguide coupling efficiency is 36%. Since the tapering length for our nanowires is short, the coupling efficiency is similar for both forward and backward directions (~18% for each direction).

We transfer preselected high quality nanowire QDs on silicon chips using a nanomanipulator. Our setup is a modified version of previous works.[33,34] It consists of a tungsten tip mounted on an x−y−z movable stage imaged by a high resolution optical microscope. The nanowire is detached at its base from the growth chip, then due to van der Waals forces it adheres to the tungsten tip. The nanowire is then transferred to a silicon chip with <500 nm position and <2 degrees rotation precision. Inset 1 of Figure 2a was captured while a nanowire was being transferred using a nanomanipulator. The chip was prepared with 2.4 μm of buried silicon oxide serving as a low index buffer between the SiN waveguide and Si substrate, as well as prefabricated markers to align the photonic circuit with respect to the nanowire. These markers allow for very precise alignment of the nanowires within the waveguide circuits (<50 nm if required). After the nanowire transfer process we encapsulate the nanowire in SiN, which acts as the core of the photonic channel. The photonic circuits are patterned and etched with respect to the alignment features and finally cladded with PMMA for symmetric mode confinement (see Supporting Information Note.1). Figure 2a shows a color coded microscope image of a single nanowire positioned within a SiN waveguide.

An important milestone toward monolithic integration of quantum optical circuits is to operate and link multiple on-chip sources. Using our method, it is possible to preselect many quantum emitters, transfer them to a silicon chip, embed them in waveguide material, select the desired ones (in terms of

DOI: 10.1021/acs.nanolett.5b04709
Nano Lett. 2016, 16, 2289−2294

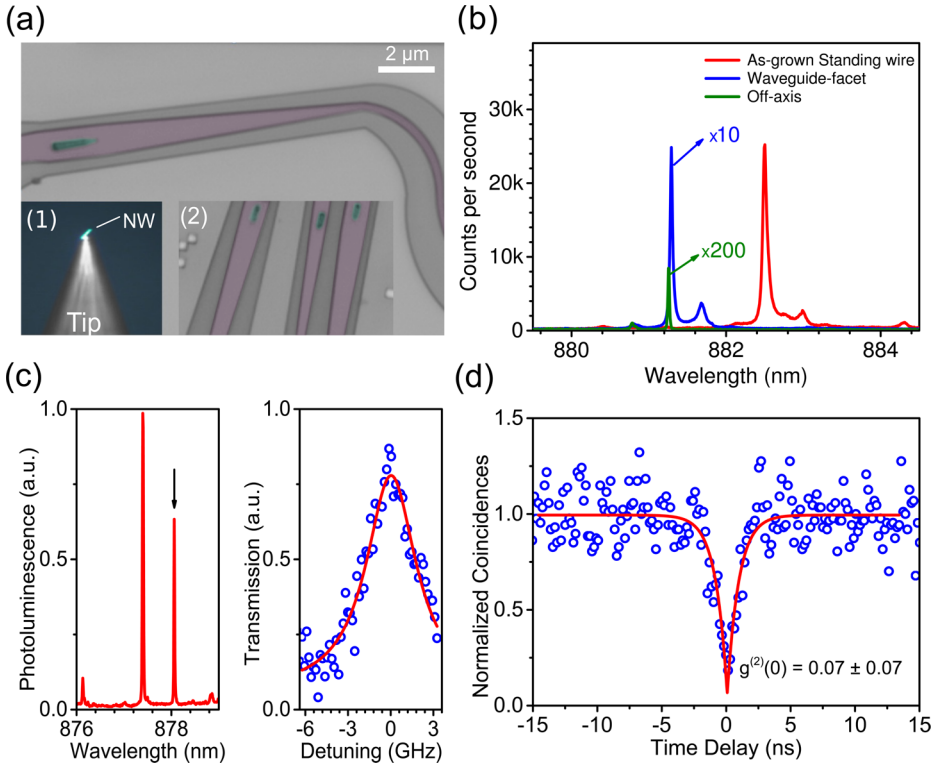

Figure 2. (a) Color coded microscope image of a single nanowire (green) integrated in a photonic waveguide (purple). Inset 1 shows a single nanowire attached to the tip of the nanomanipulator used during the nanowire transfer process. Inset 2 shows multiple selected nanowires coupled to different photonic channels. (b) Emission spectrum of a standing as-grown nanowire sample (red), its spectrum after encapsulation captured perpendicular to its growth axis (green), and finally, its emission collected from the end-facet of the SiN waveguide (blue). The emission is blue-shifted after nanowire transfer and encapsulation in SiN due to strain. (c) A scanning Fabry Pérot measurement (right) for an emission line from a nanowire QD indicated by the arrow (left). The Lorentzian fit shows a narrow line width with a FWHM of 3.45 ± 0.48 GHz ($\Delta\lambda$ = ~0.009 nm). (d) Second-order correlation measurement showing multiphoton emission probability as low as 0.07 ± 0.07.

emission wavelength, intensity, line width, etc.), and then route their emission to different input ports of photonic circuits. Inset 2 of Figure 2a shows an optical microscope image of multiple quantum emitters integrated on the same photonic circuit (Supporting Information Note.3 and Note.4). Together with electrical[35] and strain tuning[36] of nanowires, our approach allows for complex fully integrated quantum circuits.

Figure 2b compares the emission spectra of a nanowire QD before and after processing. The red spectrum originates from the as-grown nanowire QD sample collected from the nanowire tip, the green curve is the emission spectrum of the encapsulated nanowire QD captured perpendicular to its growth axis, and the blue curve is the spectrum collected from the waveguide-facet. As observed in Figure 2b, even without taking the facet-loss into account, the collected light intensity from the waveguide-facet is ~60 times higher than the off-axis QD emission. This large difference is due to the high mode matching between the electric dipole moment of the QD and the fundamental modes of the waveguide. The peak intensity of the QD emission measured from the waveguide-facet is 10% of its intensity as measured when the nanowire was still standing on the original growth chip (as-grown). We attribute this decrease to the coupling loss from the nanowire into the waveguide, the propagation loss in the waveguide and the waveguide-facet loss. After transfer and deposition of SiN, the QD emission is 1.5 nm (2.4 meV) blue-shifted due to strain.[37] We note that the small difference in the emission wavelength between the blue and green spectra is attributed to the difference in temperature of the two different mounts used for on-axis and off-axis measurements.

Sources with long coherence time and high single-photon emission probability are required for LOQC. To verify the high optical quality of our integrated sources, we carried out a scanning Fabry Pérot measurement on an emission line of an encapsulated QD presented in the left panel of Figure 2c. The right panel of Figure 2c shows the measurement results. A Lorenztian fit on the transmission spectra yields a FWHM of 3.45 ± 0.48 GHz. This value is a factor of ~7 larger than the Fourier-transform limit. The line width can be improved by resonant excitation[38] and further cooling of the sample.[39] In addition, we performed an autocorrelation measurement using continuous wave excitation at 632.8 nm to determine the single-photon purity of the photons guided along the photonic circuit. The results are presented in Figure 2d. A multiphoton emission probability of $g^2(0)$ = 0.07 ± 0.07 was measured. Furthermore, from the fitted data, we estimate an emission lifetime of T_1 = 0.9 ± 0.1 ns. These results show the high emission quality of the integrated sources, despite several processing steps including electron beam lithography, deposition, and reactive ion etching.

Our hybrid approach enables selection from a variety of materials with low propagation losses for the waveguide. Shown in Figure 3a, we measured the propagation loss for both TE and TM modes of our waveguide using the cut-back method[40] to be 4.0 ± 0.3 and 2.5 ± 0.4 dB/cm, respectively. This measurement was conducted using a tunable laser at 880 nm to match the quantum dot emission. The higher loss for TE is attributed to

DOI: 10.1021/acs.nanolett.5b04709
Nano Lett. 2016, 16, 2289−2294

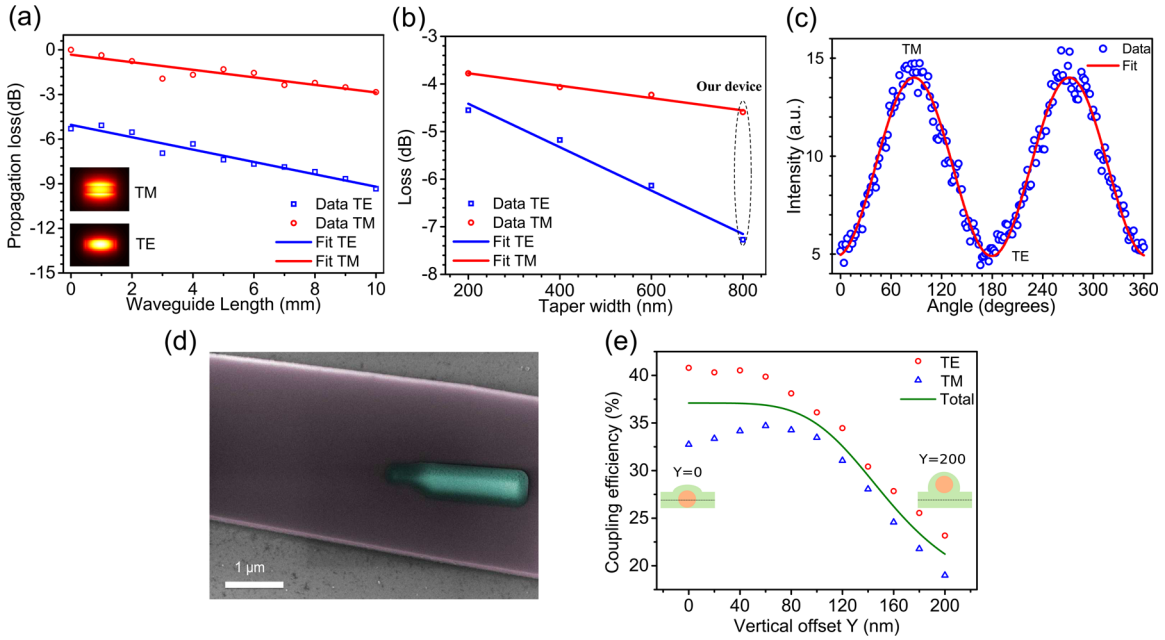

Figure 3. (a) Measurement of propagation losses for TE and TM modes using the cut-back method. TM and TE modes propagation losses are 2.5 ± 0.4 and 4.0 ± 0.3 dB/cm, respectively. (b) Waveguide-facet losses for TE and TM modes versus waveguide width at the end-facet. (c) Polarization measurement on the collected photons from the waveguide-facet. (d) Colored SEM image of the nanowire-waveguide device. Shown in purple is the SiN waveguide. The nanowire (white) in covered with a layer of SiN (green). The nanowire is shifted vertically from the center of the SiN waveguide due to the nature of the PECVD process. (e) Simulated coupling efficiency for TE and TM photons emitted from the QD as a function of the vertical offset Y of the nanowire from the center of the waveguide core. As shown in the two insets, a centered nanowire corresponds to $Y = 0$, while for a nanowire lying on top of the waveguide $Y = 200$ nm.

the larger overlap with the etched sidewalls as compared to TM. Additionally, we characterized the facet losses of TE and TM modes for different waveguide widths at the facet as shown in Figure 3b. For our device, highlighted in Figure 3b, the measured facet loss is 7.2 and 4.5 dB for TE and TM modes, respectively.

We studied the emission intensity as a function of polarization, shown in Figure 3c. Expected from the large difference in the facet loss for TE and TM modes, our source appears partially polarized. The facet losses can be improved by reducing the waveguide width adiabatically[41] to closely match the TM and TE modes to the collection objective. As shown in Figure 3b, for a 200 nm waveguide width at the facet, the difference in TE and TM facet losses falls below 0.7 dB and the total loss improves by ∼2 dB as compared to our current device. This enhanced collection efficiency for smaller taper width is similar to the case of as-grown nanowires,[42] where the tapered section of the nanowire is used for mode conversion and improving the extraction efficiency.

Taking into account the waveguide losses and comparing the emission spectra from the encapsulated device and from the as-grown sample, we estimate a unidirectional nanowire QD to waveguide coupling efficiency of ∼12.2 ± 1.7% (∼24.3% for both forward and backward directions, Supporting Information Note.5). The unidirectional coupling efficiency is smaller than the theoretical value of 18%. To better understand the remaining mechanisms for coupling loss, a scanning electron microscope image of one of the devices is presented in Figure 3d. As is observed, the nanowire is not embedded at the center of the photonic channel. During the deposition of PECVD SiN, due to the gaseous process, material builds up isotropically on all surfaces. This lifts-up the nanowire from the substrate, reducing the overlap between the electronic transition dipole moment of the QD and the electric field of the supported waveguide optical modes. We calculate the coupling efficiency as a function of vertical displacement of the nanowire with respect to the waveguide center. The results are shown in Figure 3e. The total simulated bidirectional coupling efficiency for unpolarized light varies from ∼36% for a perfectly centered wire to ∼22% for a wire that is lying on top of the waveguide (no geometrical overlap). The coupling is slightly stronger for the TE mode than the TM mode because of the asymmetric geometry of the waveguide. To avoid nanowire displacement, one can combine the PECVD process with a thin sputtered layer of SiN to anchor the nanowires on the substrate. Alternatively, other high quality sputtered waveguide technologies like aluminum nitride[43] can be used.

High system efficiency is vital for many applications in quantum optics.[44] Therefore, to address and improve the extraction efficiency from our sources, we theoretically optimize the waveguide geometry and material. The optimized design consists of a silicon carbide (SiC) waveguide suspended in air with dimensions of 500 nm × 500 nm. The refractive index of silicon carbide is 2.6[45] at the wavelengths of interest, which provides a contrast of 1.6 with air cladding. Waveguides with loss as low as 5 dB/cm can be made using SiC films deposited by PECVD at temperatures compatible with our devices.[46] We performed 3D FDTD modeling to estimate the coupling efficiency from a nanowire QD to the guided modes of a SiC waveguide. The symmetric design of the waveguide closely matches the coupling for both orthogonal electronic dipole transitions of the QD. The coupling efficiency to each side is ∼46% (92% in total) for unpolarized light.

To produce on-demand single photons on-chip,[47] all photons must be steered in one direction. For this purpose we designed a broadband 1D mirror consisting of etched

DOI: 10.1021/acs.nanolett.5b04709
Nano Lett. 2016, 16, 2289−2294

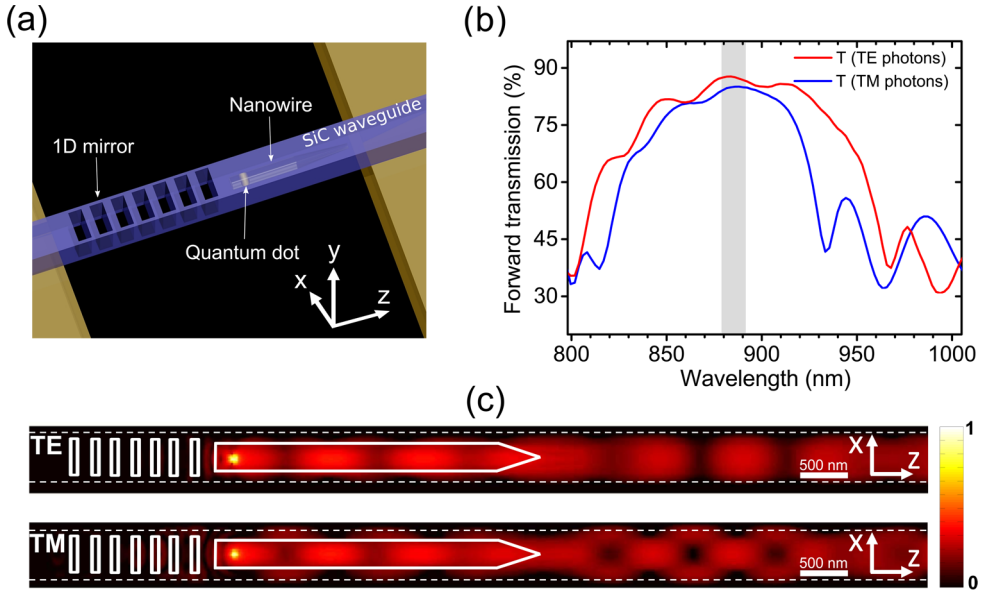

Figure 4. (a) Proposed device for efficient unidirectional coupling to a single mode waveguide from a nanowire-based QD. The device consists of a SiC waveguide with size 500 nm × 500 nm suspended in air. A 1D mirror consisting of etched squares is used to direct the photons in the forward direction of the waveguide. The etched squares have dimensions of 132 nm × 400 nm and a lattice constant of 232 nm along the *z*-direction. (b) The unidirectional coupling efficiency of the QD to waveguide calculated with 3D FDTD simulations. The total coupling efficiency is ∼92% with more than 86% for the forward propagating modes. High coupling efficiency is achieved because of high reflectivity of the mirror at the desired wavelength. (c) Electric field intensity profile of guided TE and TM modes at 880 nm. The photons are reflected by the mirror toward the right side. Dashed lines show the SiC waveguide boundaries.

squares of dimensions 132 nm × 400 nm with a lattice constant of 232 nm along the waveguide. Figure 4a illustrates the design, and Figure 4b shows the coupling efficiency as a function of wavelength. The device provides a unidirectional coupling efficiency greater than 86% at 880 nm. As shown in the gray highlighted area of Figure 4b, the coupling efficiency has negligible sensitivity to polarization over the typical emission range of our QDs. The polarization-insensitive high coupling efficiency combined with symmetric waveguide geometry make our device ideal for experiments with polarization-entangled photons. Figure 4c represents the electric field intensity profile of guided TE and TM modes at 880 nm.

In summary, we have demonstrated controlled integration of preselected nanowire-based single quantum emitters into photonic waveguides. Our novel technique enables scalable integration of selected sources in complex photonic architectures on a single chip. The integrated sources maintain their high optical quality in terms of single photon purity, line width, and intensity with a coupling efficiency to the photonic waveguide as high as 24%. Furthermore, we showed theoretically that for a suspended SiC waveguide, in conjunction with a 1D Bragg reflector, a unidirectional coupling efficiency greater than 86% can be realized. Coupling our quantum emitters to on-chip photonic cavities will allow to investigate the rich physics of cavity quantum electrodynamics, thus enhancing the spontaneous emission rate to accelerate the emission lifetime and approach Fourier-transform limited photons. Finally, by local tuning of the emission energy of single photon sources, indistinguishable photons can be generated as a necessary step toward on-chip optical quantum computation.

■ ASSOCIATED CONTENT

Ⓢ Supporting Information

The Supporting Information is available free of charge on the ACS Publications website at DOI: 10.1021/acs.nanolett.5b04709.

Details about fabrication (Note.1), the experimental setup (Note.2), additional examples of functional devices (Note.3 and Note.4), and efficiency calculation (Note.5) (PDF)

■ AUTHOR INFORMATION

Corresponding Authors

*E-mail: i.esmaeilzadeh@tudelft.nl.

*E-mail: elshaari@kth.se. Phone: +46 (0)8 5537 8000.

Author Contributions

⊥These authors contributed equally to this work.

Notes

The authors declare no competing financial interest.

■ ACKNOWLEDGMENTS

This research was supported by the Dutch Foundation for Fundamental Research on Matter (FOM projectruimte 10NQO02 and 12PR2994) and the European Union Seventh Framework Program 209 (FP7/2007-2013) under Grant Agreement No. 601126 210 (HANAS). K.D.J. acknowledges funding from the MARIE SKŁODOWSKA-CURIE Individual Fellowship under REA grant agreement No. 661416 (SiPhoN). M.E.R acknowledges funding from Industry Canada.

■ REFERENCES

(1) Knill, E.; Laflamme, R.; Milburn, G. J. *Nature* **2001**, *409*, 46−52.
(2) O'Brien, J. L.; Pryde, G. J.; White, A. G.; Ralph, T. C.; Branning, D. *Nature* **2003**, *426*, 264−267.

DOI: 10.1021/acs.nanolett.5b04709
Nano Lett. 2016, 16, 2289−2294

(3) Gasparoni, S.; Pan, J.-W.; Walther, P.; Rudolph, T.; Zeilinger, A. *Phys. Rev. Lett.* **2004**, *93*, 020504.
(4) Yao, X.-C.; Wang, T.-X.; Ping, J. X.; He, X.-H. B.; Pan, G.-S.; Peng, C.-Z.; Chen, C.-Y.; Pan, J.-W. *Nat. Photonics* **2012**, *6*, 225−228.
(5) Politi, A.; Cryan, M. J.; Rarity, J. G.; Yu, S.; O'Brien, J. L. *Science* **2008**, *320*, 646−649.
(6) Politi, A.; Matthews, J. C. F.; O'Brien, J. L. *Science* **2009**, *325*, 1221.
(7) Sansoni, L.; Sciarrino, F.; Vallone, G.; Mataloni, P.; Crespi, A.; Ramponi, R.; Osellame, R. *Phys. Rev. Lett.* **2010**, *105*, 200503.
(8) Peruzzo, A.; Shadbolt, P.; Brunner, N.; Popescu, S.; O'Brien, J. L. *Science* **2012**, *338*, 634−637.
(9) Spring, J. B.; Metcalf, B. J.; Humphreys, P. C.; Kolthammer, S. W.; Jin, X.-M.; Barbieri, M.; Datta, A.; Thomas-Peter, N.; Langford, N. K.; Kundys, D.; Gates, J. C.; Smith, B. J.; Smith, P. G. R.; Walmsley, I. A. *Science* **2013**, *339*, 798−801.
(10) Müller, M.; Bounouar, S.; Jöns, K. D.; Glässl, M.; Michler, P. *Nat. Photonics* **2013**, *8*, 224−228.
(11) Gerardot, B. D.; Seidl, S.; Dalgarno, P. A.; Warburton, R. J.; Granados, D.; Garcia, J. M.; Kowalik, K.; Krebs, O.; Karrai, K.; Badolato, A.; Petroff, P. M. *Appl. Phys. Lett.* **2007**, *90*, 041101.
(12) Bennett, A. J.; Pooley, M. A.; Stevenson, R. M.; Ward, M. B.; de la Giroday, A. B.; Sköld, N.; Farrer, I.; Nicoll, C. A.; Ritchie, D. A.; Shields, A. J. *Nat. Phys.* **2010**, *6*, 947−950.
(13) Seidl, S.; Kroner, M.; Högele, A.; Karrai, K.; Warburton, R. J.; Badolato, A.; Petroff, P. M. *Appl. Phys. Lett.* **2006**, *88*, 203113.
(14) Rastelli, A.; Ding, F.; Plumhof, J. D.; Kumar, S.; Trotta, R.; Deneke, C.; Malachias, A.; Atkinson, P.; Zallo, E.; Zander, T.; et al. *Phys. Status Solidi B* **2012**, *249*, 687−696.
(15) Trotta, R.; Martin-Sanchez, J.; Wildmann, J. S.; Piredda, G.; Reindl, M.; Schimpf, C.; Zallo, E.; Stroj, S.; Edlinger, J.; Rastelli, A. *Nat. Commun.* **2016**, *7*, 10375.
(16) Yuan, Z.; Kardynal, B. E.; Stevenson, R. M.; Shields, A. J.; Lobo, C. J.; Cooper, K.; Beattie, N. S.; Ritchie, D. A.; Pepper, M. *Science* **2002**, *295*, 102−105.
(17) Reck, M.; Zeilinger, A.; Bernstein, H. J.; Bertani, P. *Phys. Rev. Lett.* **1994**, *73*, 58−61.
(18) Lipson, M. *J. Lightwave Technol.* **2005**, *23*, 4222−4238.
(19) Marsili, F.; Verma, V. B.; Stern, J. A.; Harrington, S.; Lita, A. E.; Gerrits, T.; Vayshenker, I.; Baek, B.; Shaw, M. D.; Mirin, R. P.; Nam, S. W. *Nat. Photonics* **2013**, *7*, 210−214.
(20) Pernice, W.; Schuck, C.; Minaeva, O.; Li, M.; Goltsman, G.; Sergienko, A.; Tang, H. *Nat. Commun.* **2012**, *3*, 1325.
(21) Schuck, C.; Pernice, W. H. P.; Tang, H. X. *Appl. Phys. Lett.* **2013**, *102*, 051101.
(22) Martin-Lopez, E.; Laing, A.; Lawson, T.; Alvarez, R.; Zhou, X.-Q.; O'Brien, J. L. *Nat. Photonics* **2012**, *6*, 773−776.
(23) Carolan, J.; Harrold, C.; Sparrow, C.; Martín-López, E.; Russell, N. J.; Silverstone, J. W.; Shadbolt, P. J.; Matsuda, N.; Oguma, M.; Itoh, M.; et al. *Science* **2015**, *349*, 711−716.
(24) Badolato, A.; Hennessy, K.; Atatüre, M.; Dreiser, J.; Hu, E.; Petroff, P. M.; Imamoğlu, A. *Science* **2005**, *308*, 1158−1161.
(25) Claudon, J.; Bleuse, J.; Malik, N. S.; Bazin, M.; Jaffrennou, P.; Gregersen, N.; Sauvan, C.; Lalanne, P.; Gerard, J.-M. *Nat. Photonics* **2010**, *4*, 174−177.
(26) Makhonin, M. N.; Dixon, J. E.; Coles, R. J.; Royall, B.; Luxmoore, I. J.; Clarke, E.; Hugues, M.; Skolnick, M. S.; Fox, A. M. *Nano Lett.* **2014**, *14*, 6997−7002. , PMID: 25381734
(27) Reithmaier, G.; Lichtmannecker, S.; Reichert, T.; Hasch, P.; Müller, K.; Bichler, M.; Gross, R.; Finley, J. J. *Sci. Rep.* **2013**, *3*, 1901.
(28) Jöns, K. D.; Rengstl, U.; Oster, M.; Hargart, F.; Heldmaier, M.; Bounouar, S.; Ulrich, S. M.; Jetter, M.; Michler, P. *J. Phys. D: Appl. Phys.* **2015**, *48*, 085101.
(29) Prtljaga, N.; Coles, R. J.; O'Hara, J.; Royall, B.; Clarke, E.; Fox, A. M.; Skolnick, M. S. *Appl. Phys. Lett.* **2014**, *104*, 231107.
(30) Reithmaier, G.; Senf, J.; Lichtmannecker, S.; Reichert, T.; Flassig, F.; Voss, A.; Gross, R.; Finley, J. J. *J. Appl. Phys.* **2013**, *113*, 143507.
(31) Mouradian, S. L.; Schröder, T.; Poitras, C. B.; Li, L.; Goldstein, J.; Chen, E. H.; Walsh, M.; Cardenas, J.; Markham, M. L.; Twitchen, D. J.; Lipson, M.; Englund, D. *Phys. Rev. X* **2015**, *5*, 031009.
(32) Dalacu, D.; Mnaymneh, K.; Lapointe, J.; Wu, X.; Poole, P. J.; Bulgarini, G.; Zwiller, V.; Reimer, M. E. *Nano Lett.* **2012**, *12*, 5919−5923.
(33) Wolters, J.; Schell, A. W.; Kewes, G.; Nüsse, N.; Schoengen, M.; Döscher, H.; Hannappel, T.; Löchel, B.; Barth, M.; Benson, O. *Appl. Phys. Lett.* **2010**, *97*, 141108.
(34) Benyoucef, M.; Kiravittaya, S.; Mei, Y. F.; Rastelli, A.; Schmidt, O. G. *Phys. Rev. B: Condens. Matter Mater. Phys.* **2008**, *77*, 35108.
(35) Reimer, M. E.; van Kouwen, M. P.; Hidma, A. W.; van Weert, M. H. M.; Bakkers, E. P. A. M.; Kouwenhoven, L. P.; Zwiller, V. *Nano Lett.* **2011**, *11*, 645−650. , PMID: 21226507
(36) Kremer, P. E.; Dada, A. C.; Kumar, P.; Ma, Y.; Kumar, S.; Clarke, E.; Gerardot, B. D. *Phys. Rev. B: Condens. Matter Mater. Phys.* **2014**, *90*, 201408.
(37) Bavinck, M. B.; Zieliński, M.; Witek, B. J.; Zehender, T.; Bakkers, E. P. A. M.; Zwiller, V. *Nano Lett.* **2012**, *12*, 6206−6211.
(38) Kuhlmann, A. V.; Prechtel, J. H.; Houel, J.; Ludwig, A.; Reuter, D.; Wieck, A. D.; Warburton, R. J. *Nat. Commun.* **2015**, *6*, 8204.
(39) Reimer, M. E.; Bulgarini, G.; Heeres, R.; Witek, B. J.; Versteegh, M. A. M.; Dalacu, D.; Lapointe, J.; Poole, P. J.; Zwiller, V. ArXiv e-prints, 2014.
(40) Vlasov, Y.; McNab, S. *Opt. Express* **2004**, *12*, 1622−1631.
(41) Almeida, V. R.; Panepucci, R. R.; Lipson, M. *Opt. Lett.* **2003**, *28*, 1302−1304.
(42) Reimer, M. E.; Bulgarini, G.; Akopian, N.; Hocevar, M.; Bavinck, M. B.; Verheijen, M. A.; Bakkers, E. P.; Kouwenhoven, L. P.; Zwiller, V. *Nat. Commun.* **2012**, *3*, 737.
(43) Xiong, C.; Pernice, W. H. P.; Sun, X.; Schuck, C.; Fong, K. Y.; Tang, H. X. *New J. Phys.* **2012**, *14*, 095014.
(44) Kok, P.; Munro, W. J.; Nemoto, K.; Ralph, T. C.; Dowling, J. P.; Milburn, G. J. *Rev. Mod. Phys.* **2007**, *79*, 135−174.
(45) Singh, S.; Potopowicz, J. R.; Uitert, L. G. V.; Wemple, S. H. *J. Appl. Phys.* **1971**, *19*, 53−56.
(46) Shoji, Y.; Nakanishi, K.; Sakakibara, Y.; Kintaka, K.; Kawashima, H.; Mori, M.; Kamei, T. *Appl. Phys. Express* **2010**, *3*, 122201.
(47) Söllner, I.; Mahmoodian, S.; Hansen, S. L.; Midolo, L.; Javadi, A.; Kiranskė, G.; Pregnolato, T.; El-Ella, H.; Lee, E. H.; Song, J. D.; Stobbe, S.; Lodahl, P. *Nat. Nanotechnol.* **2015**, *10*, 775−778.

DOI: 10.1021/acs.nanolett.5b04709
Nano Lett. 2016, 16, 2289−2294